ACS OMEGA

Open Access

http://pubs.acs.org/journal/acsodf

Article

Theoretical Study on the Structural, Mechanical, Thermodynamic, and Vibrational Properties of $Ti_8Ni_{8-x}Fe_x$ (X = 0−8) Shape Memory Alloys for Biomedical Applications

Thabiso Mathews,* Enoch Sithole, Rosinah Modiba, and Mandy Madigoe

Cite This: *ACS Omega* 2025, 10, 18303−18311

Read Online

ACCESS | Metrics & More | Article Recommendations | Supporting Information

ABSTRACT: Shape Memory Alloys (SMAs) are metal alloys that can return to their original shape after deforming. In this study, Density Functional Theory (DFT) has been employed to study the structural, mechanical, thermodynamic, and vibrational properties of $Ti_8Ni_{8-x}Fe_x$ SMAs, with Fe content varying from x = 0 to 8. Calculated lattice parameters agreed well with the theoretical and experimental data, confirming the validity of this study. The structural analysis revealed a decrease in formation energy with increasing Fe content. These indicated the enhancement of the thermodynamic stability of the alloys. The calculated mechanical property showed a decrease in Poisson's ratio as the Fe content increased, suggesting that the SMAs transit toward brittle behavior. Similarly, the G/B ratio was found to increase, confirming an improvement in the resistance to plastic deformation. The addition of Fe enhances C' values and decreases the anisotropy of the alloys. Phonon dispersion calculations were conducted to evaluate the vibrational stability of the alloys. The results indicated that Fe doping modifies the elastic properties and influences the alloy's mechanical performance. Fe contents changed the phonon frequencies due to bonding characteristics between Ni and Fe. Vibrational instability has been observed for $Ti_8Ni_{8-x}Fe_x$ (x = 0−2), while (x = 3−7) demonstrated the vibrational stability of the alloys. The $Ti_8Ni_1Fe_7$ alloy is the most thermodynamically stable and is a promising candidate for biomedical applications.

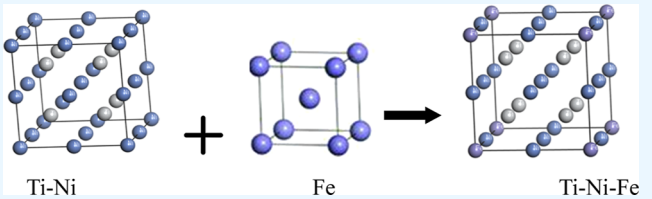

1. INTRODUCTION

Shape memory alloys (SMAs) have drawn an enormous amount of attention since their discovery in the 1930s because of their distinctive functional characteristics, such as the shape memory effect (SME) and superelasticity (SE), a class of martensitic transformation (MT).[1,2] These unique properties enable the development of innovative technologies. SMAs have a wide range of potential applications in aviation and space travel, ocean development, mechanics, electronics, robotics, automation, and medical devices.[3,4] Titanium−nickel (TiNi) SMA is often used in medical devices, due to its lower Young's modulus property.[4] TiNi is regarded as the near-equal atomic SMA with phase transition from a cubic B2 structure to a monoclinic $B19'$ phase.[5] The MT between a high-temperature B2 austenite phase and a low-temperature $B19'$ martensite phase is the fundamental mechanism of SME behavior. The MT in SMAs is brought by the presence of soft modes and instabilities in the austenite phase.[6] The austenitic phase is highly symmetrical at high temperatures, while the martensitic phase is less symmetrical at lower temperatures. The martensitic phase can be divided into stress-free and stress-induced martensite. The transformation between austenite and martensite is driven by a stress-temperature function, leading to a thermoelastic martensitic transformation (TMT) that occurs without thermal diffusion.[7]

A biomaterial refers to a substance, either of biological or synthetic origin, that can be used in the human body as a component of a medical device or as a substitute for an organ or physiological process. It is commonly used in dental and orthopedic implants. The biocompatibility of a material refers to its capacity to induce an appropriate response from the host organism. An optimal biomaterial should possess exceptional resistance to corrosion within the physiological environment of the human body. It should also exhibit a chemically compatible composition to mitigate any unfavorable reactions with bodily tissues. The safety and reliability of medical devices are important for long-term implants in clinical medical applications. The corrosion of TiNi alloys in biomedical applications poses challenges that can affect the safety and performance of the devices. However, proteins and amino acids found in bodily fluids hasten metal corrosion and encourage the release of poisonous nickel ions.[4]

The orthopedic implantation applications, osteoporosis, arise from the "stress shielding", which causes bone resorption

Received: September 30, 2024
Revised: April 7, 2025
Accepted: April 14, 2025
Published: April 30, 2025

associated with implants since the load cannot be transferred from the implants to the surrounding bone tissues. Porous NiTi SMAs thus become hard-tissue implantable, or replacement materials, due to their low modulus and the ability to exchange bodily fluids, promote cell adhesion and in-growth, and lower and match the elastic modulus with different hard tissues.[8] Furthermore, metallic ion release impairs osseointegration and ultimately results in clinical failure.[9] likewise, the weak osteoinductive properties of TiNi SMAs indicate that these molecules have not yet been optimized for biomedical applications. For certain physiological environments, the smooth and hydrophobic surface properties of TiNi alloys do not provide a cell-friendly scaffold. Surface roughness is important for cell binding. Previous research has shown that a high-texture surface is the best design for an implant with desirable osseointegration.[10]

Corrosion resistance and surface biocompatibility of titanium−nickel alloy surfaces must be modified. The starting temperature of MT Ms, of TiNi alloys, decreases after Ni substitution with V, Cr, Mn, Fe, or Co but increases noticeably after Ni substitution with Au, Pd, Zr, or Pt in amounts not less than 15−20 at % and adding Co increases the yield strength.[11] Pushin and his colleagues listed the effects of binary and near equiatomic nitinol on transition temperature.[12] The strong concentration dependence of the start (Ms, As) and finish (Mf, Af) temperatures of the forward and reverse thermoelastic diffusion caused changes in the chemical composition of binary TiNi alloys with the SMEs between 50.0 and 51.2 at % Ni. Therefore, it has been proposed that β-type alloys are stronger and have a lower modulus of elasticity than α and $(\alpha + \beta)$-type alloys.[13,14] On the other hand, nontoxic β-stabilizer elements (such as Nb, Ta, Zr, and Mo) have been extensively studied for metallic implants.[15]

The study of $Ti_8Ni_{8-x}Fe_x$ alloys was motivated by the fact that TiNi alloys exhibit good corrosion resistance under physiological conditions. Therefore, adding Fe atoms to the TiNi alloy can fine-tune the MT temperature, enabling the alloy to function effectively at body temperature and enhancing the material's durability. Fe has the potential to improve the strength and stiffness of the material, enabling matching with tissue to minimize stress shielding. These properties make TiNiFe alloys a promising candidate for biomedical devices. This study aims to address the gap in understanding how chemical modifications influence the MT temperature and mechanical behavior of TiNi SMAs in biomedical applications. TiNi alloys are known for their shape memory and pseudoelastic properties, which often deviate from the optimal range for use in the human body. Substituting Fe atoms seeks to fine-tune temperature and enhance TiNi performance. Therefore, the purpose of this study was to investigate the impact of substituting Ni with Fe on the shape memory properties of TiNi alloy using a first-principles methodology for biomedical applications.

2. METHODOLOGY

The computations were carried out utilizing the Cambridge Sequence Total Energy Package (CASTEP) code[16,17] that uses Density Functional Theory (DFT) with the generalized gradient approximation (GGA) of Perdew, Burke, and Ernzerhof (PBE).[18] The convergence tolerances of energy, maximum force, maximum stress, and maximum displacement have been set to 1.0×10^6 eV/atom, 0.03 eV/Å, 0.05 GPa, and 0.001 Å, respectively. The cutoff energy was selected at 500 eV to ensure a high accuracy. The self-consistent field (SCF) tolerance was 1.0×10^6 eV/atom. A suitable k-point sampling of the Monkhorst−Pack grid with an $8 \times 8 \times 8$ k-point mesh was used to approximate the Brillouin zone. Ultrasoft pseudopotentials were employed to convey all of the ions. DFT was used to compute the phonon characteristics and assess the phonon dispersion spectra. By minimizing forces and stress tensors, structural parameters (atomic locations and lattice parameters) were optimized. The finite displacement method was used. The force constants for the phonon dispersions were obtained by using a supercell technique. For B2 structures, a $2 \times 2 \times 2$ supercell (16 atoms) has been employed.[19]

Figure 1 shows (a) undoped Ti_8Ni_8 structure and (b) doped $Ti_8Ni_{8-x}Fe_x$ structure, where x = 0−8. Ti_8Ni_8 is a cubic B2 structure with a $Pm\bar{3}m$ space group. The TiNi arrangement was replicated using the Supercell Method (SM), where a supercell of 16 atoms was built and Ni atoms were substituted with (1−8) atoms of Fe. All crystal structures have been optimized as monoclinic structures.

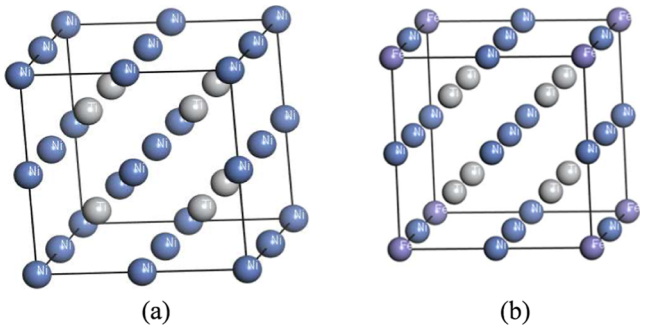

Figure 1. The crystal structure of (a) undoped Ti_8Ni_8 and (b) doped $Ti_8Ni_{8-x}Fe_x$ (x = 0−8).

The BFGS algorithm was used for geometrically optimizing the doped alloys. The valence electron configuration used in the optimization calculation was as follows: Ti is $3d^24s^2$, Ni is $3d^84s^2$, and Fe is $3d^64s^2$. Elements close in atomic size to Ni were distributed in austenite to stabilize the γ matrix.[20,21]

3. RESULTS AND DISCUSSION

3.1. Structural, Heats of Formation, and Elastic Constants for $Ti_8Ni_{8-x}Fe_x$. An investigation using first-principles computation was conducted to gain a deeper comprehension of the impact of Fe substitution on the thermodynamic stability of the TiNi crystal structure. Table 1 lists the computed lattice parameter, the heat of formation, and elastic constants (C_{ij}) of $Ti_8Ni_{8-x}Fe_x$ (x = 0−8). The calculated values are compared to results obtained from experimental and theoretical values in the literature. The DFT calculations replicate identical TiNi lattice constant and heat formation. The calculated lattice parameter of the equiatomic TiNi was determined to be 3.015 Å in close agreement with theoretical and experimental values.[22−25] When Ni is replaced with Fe, the lattice parameter of TiNi decreases. This is attributed to different atomic radii, Ni (0.163 nm) and Fe (0.126 nm). The heat of formation was computed using eq 1

$$\Delta E = \frac{Ti_8Ni_{8-x}Fe_x}{16} - \sum\left(\frac{8}{16}E_{Ti} + \frac{8-x}{16}E_{Ni} - \frac{x}{16}E_{Fe}\right) \quad (1)$$

https://doi.org/10.1021/acsomega.4c08953
ACS Omega 2025, 10, 18303−18311

Table 1. Calculated Lattice Parameters ($a = b = c$), Heats of Formation (ΔH_f), and Elastic Constants (C_{ij})

structure	$a = b = c$ (Å)	ΔH_f (eV/atom)	C_{11} (GPa)	C_{12} (GPa)	C_{44} (GPa)	C' (GPa)	A (GPa)
TiNi[23]	3.016	−0.380			59.00	33.00	
TiNi[26]	3.020	−0.410					
TiNi[24]	3.011	−0.403	190.32	143.97	58.36	23.18	2.52
TiNi[25]	3.014		162.00	132.00	36.00	15.00	2.40
$Ti_8Ni_7Fe_1$	3.005	−0.434	186.78	167.36	52.78	9.71	5.44
$Ti_8Ni_6Fe_2$	2.995	−0.459	188.11	157.39	61.42	15.37	3.99
$Ti_8Ni_5Fe_3$	2.985	−0.488	195.46	153.51	63.47	20.98	3.03
$Ti_8Ni_4Fe_4$	2.98	−0.529	230.04	136.69	63.12	46.68	1.35
$Ti_8Ni_3Fe_5$	2.97	−0558	254.42	131.36	71.35	61.53	1.16
$Ti_8Ni_2Fe_6$	2.96	−0.600	319.32	136.42	75.45	91.45	0.83
$Ti_8Ni_1Fe_7$	2.95	−0.646	350.57	120.09	77.67	115.24	0.67
Ti_8Fe_8	2.945	−0.695	399.18	98.71	83.22	150.23	0.55

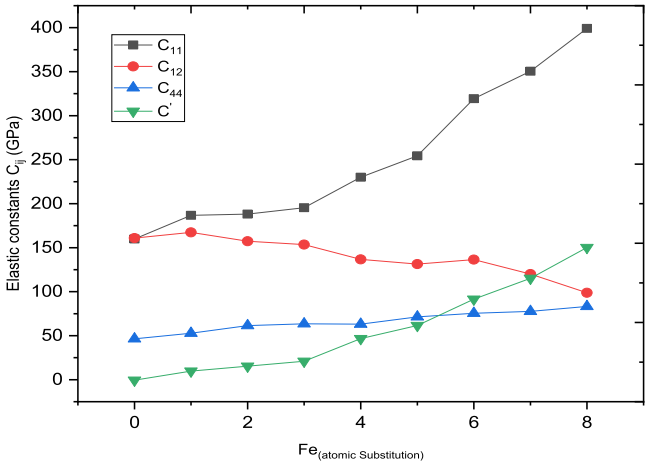

Figure 2. Elastic constants as a function of the Fe concentration.

where ΔE is the total energy of $Ti_8Ni_{8-x}Fe_x$ (x = 0−8) B2 cubic structure, and E_{Ti}, E_{Ni}, and E_{Fe} are the energies of elements. The heat of formation decreases with a rising Fe concentration. In this study, the Ti_8Fe_8 alloy was found to have the smallest heat of formation (−0.695 eV/atom), making it the most thermodynamically stable structure among the other alloys.

Elastic constants C_{ij} are used to characterize the parameters of the material resisting stress and deformation. The cubic structure has independent elastic constants, C_{11}, C_{12}, and C_{44}. Understanding the composition of the material requires an understanding of the trends of the elastic constants C_{44} and C'.[26] The crystal to be stable must satisfy eqs 2 and 3 as provided by the Born−Huang mechanical stability criteria for the cubic crystal[27]

$$C_{11} > 0, \quad C_{44} > 0, \quad (C_{11} - C_{12}) > 0 \tag{2}$$

$$(C_{11} + 2C_{12}) > 0 \tag{3}$$

The crystal's mechanical stability is indicated by the positive $\frac{C_{11} - C_{12}}{2}$. The Fe substitution for x = 0−8 has shown positive elastic constants C_{11}, C_{12}, and C_{44}, suggesting that the structures are mechanically stable. The addition of Fe enhances the C' value. When $x > 0$ at % Fe, the coupling of C_{11} and C_{12} is found, which corresponds to the observed stability trend. When $x \geq 37.5$ at %, the coupling of C_{44} and C' is also visible as seen in Figure 2, and a potential phase transition and the coupling between C_{44} and C' resulted in the $B19'$ phase.[28]

When a compound is isotropic, the (A) value is one (1); any lower or greater value denotes the degree of elastic anisotropy.[24] Furthermore, a lower transformation temperature is indicated by a lower value of A as given in eq 4

$$A = \frac{2C_{44}}{C_{11} - C_{12}} \tag{4}$$

For the B2 to $B19$ MT, the smaller A suggests a stronger correlation between C_{44} and C'. As the Fe content increases, the anisotropy value decreases. For a value greater than 0.8, the computed A could be used to assess the ductility of metals.[29] It has been observed that the calculated anisotropy values for $Ti_8Ni_{8-x}Fe_x$ (x = 0−8) are greater than 0.8, indicating ductility. The C_{44} value is comparable to the first-principles calculations.[24] The low value of C_{44} means that the shear resistance approaches the C' shear resistance, allowing both shears to occur cooperatively at the temperature of the MT, forming monoclinic martensite $B19'$.

3.2. Mechanical Properties. The substitution of nickel with iron in TiNi alloys influences the mechanical behavior of

Table 2. Bulk, Shear, Young Modulus, Poisson's Ratio, Pugh's Ratio, and Hardness

structure	B (GPa)	G (GPa)	Y (GPa)	Υ	G/B	H_v (GPa)	universal anisotropy
Ti_8Ni_8	160.61	13.17	151.83	0.46	0.08	0.26	−109.76
$Ti_8Ni_7Fe_1$	173.83	27.29	77.79	0.42	0.16	1.16	4.34
$Ti_8Ni_6Fe_2$	167.63	35.46	99.37	0.40	0.21	1.97	2.69
$Ti_8Ni_5Fe_3$	167.49	40.76	113.11	0.39	0.24	2.55	1.63
$Ti_8Ni_4Fe_4$	167.81	55.33	151.02	0.35	0.33	4.56	0.11
$Ti_8Ni_3Fe_5$	172.38	67.25	178.53	0.33	0.39	6.21	0.03
$Ti_8Ni_2Fe_6$	197.38	81.49	214.89	0.31	0.41	7.59	0.05
$Ti_8Ni_1Fe_7$	196.91	91.00	236.58	0.29	0.46	9.33	0.19
Ti_8Fe_8	198.95	105.64	269.27	0.27	0.53	12.14	0.43

https://doi.org/10.1021/acsomega.4c08953
ACS Omega 2025, 10, 18303−18311

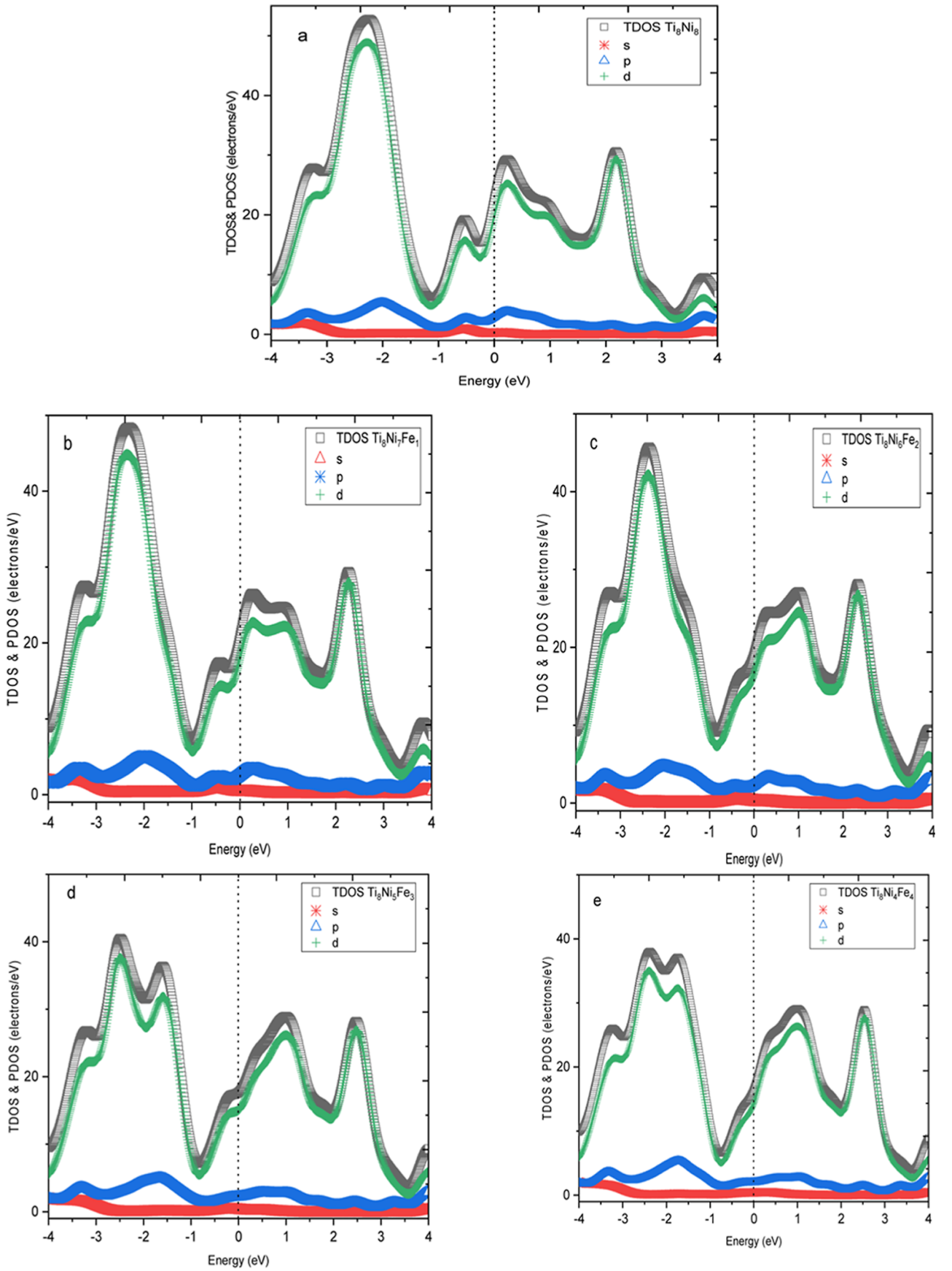

Figure 3. continued

https://doi.org/10.1021/acsomega.4c08953
ACS Omega 2025, 10, 18303−18311

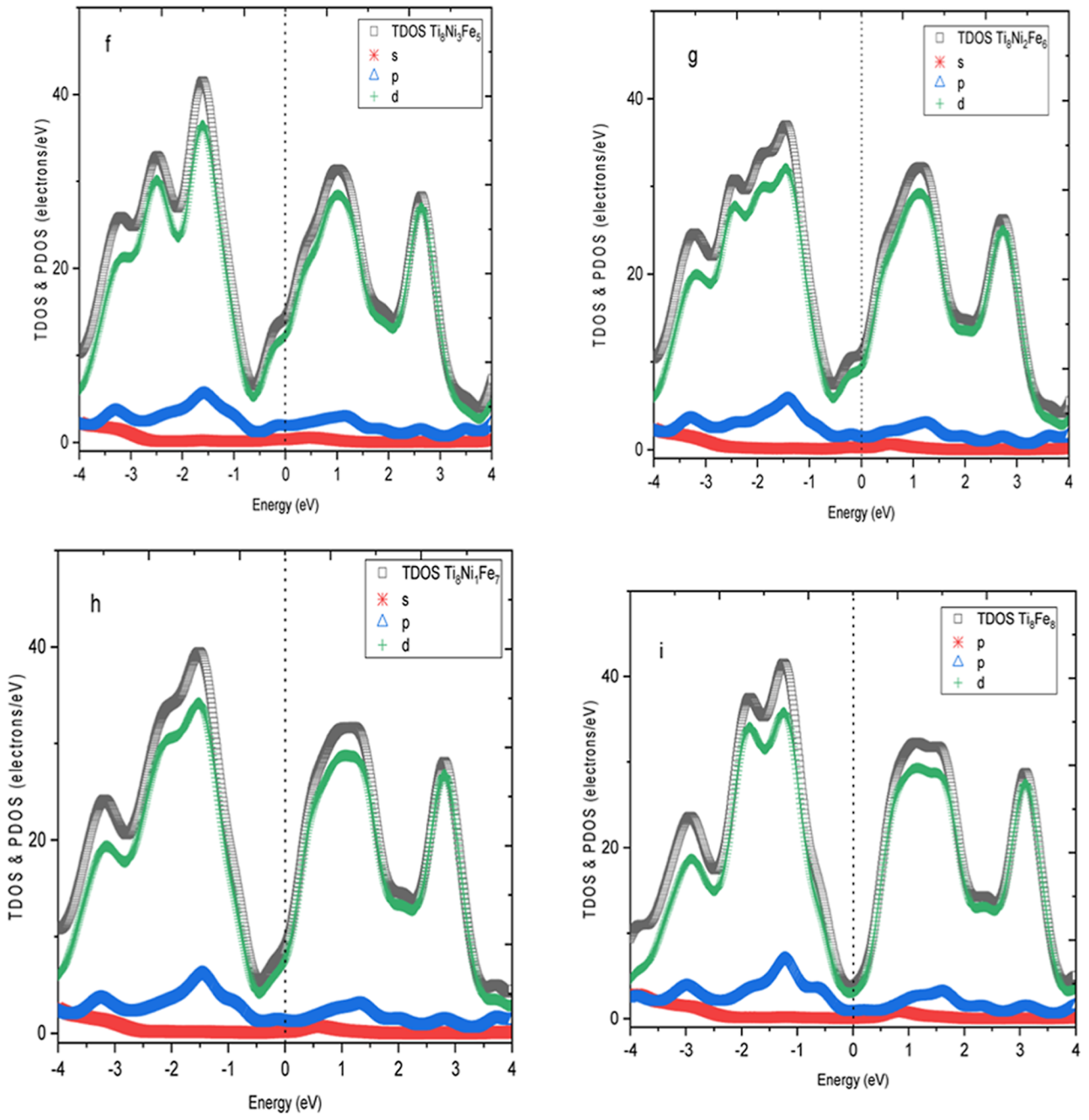

Figure 3. DOS and PDOS for (a) Ti_8Ni_8, (b) $Ti_8Ni_7Fe_1$, (c) $Ti_8Ni_6Fe_2$, (d) $Ti_8Ni_5Fe_3$, (e) $Ti_8Ni_4Fe_4$, (f) $Ti_8Ni_3Fe_5$, (g) $Ti_8Ni_2Fe_6$, (h) $Ti_8Ni_1Fe_7$, and (i) Ti_8Fe_8 alloys.

the alloys. The elasticity parameters of alloys are used to study a material's mechanical properties, including its bulk modulus, Young's modulus, shear modulus, and Poisson's ratio.[30,31] Table 2 provides Bulk (B), Shear (G), Young's (Y) Modulus, Poisson's ratio (Υ), Pugh's ratio (B/G), and Hardness H_v. The bulk modulus increases with the addition of Fe content to the TiNi alloy, suggesting that the hardness of the $Ti_8Ni_{8-x}Fe_x$ structures is improved. Ti_8Fe_8, for instance, seems to be the hardest because it has the largest bulk modulus (198.95 GPa), followed by $Ti_8Ni_1Fe_7$. Ti_8Ni_8 exhibits a lower shear moduli of 13.17 GPa, suggesting that it is brittle and compressible. The shear modulus increases with the addition of the Fe atoms, ranging from 13.17 to 105.64 GPa. This indicates that the alloy's resistance to shear deformation has been enhanced. The alloys have shown stability and ductility. The materials having large Young's modulus fall into the rigid category. Notably, $Ti_8Ni_7Fe_1$ exhibits the lowest Young's modulus value, signifying that it is the least stiff. When contrasted with other compositions, Young's modulus value increased significantly when the ratio of Fe was increased, indicating the strong stiffness of the material.

The shear capacity of the material is indicated by Poisson's ratio, in which a higher Poisson ratio indicates greater plasticity.[30,31] Poisson's ratio measures the alloy's tendency to expand in the directions perpendicular to the compression, suggesting a reduction of the alloy's ability to withstand plastic deformation. The ratio decreases with increased Fe contents. Poisson's ratio must be less than 0.35 for a ductile structure.[29]

https://doi.org/10.1021/acsomega.4c08953
ACS Omega 2025, 10, 18303−18311

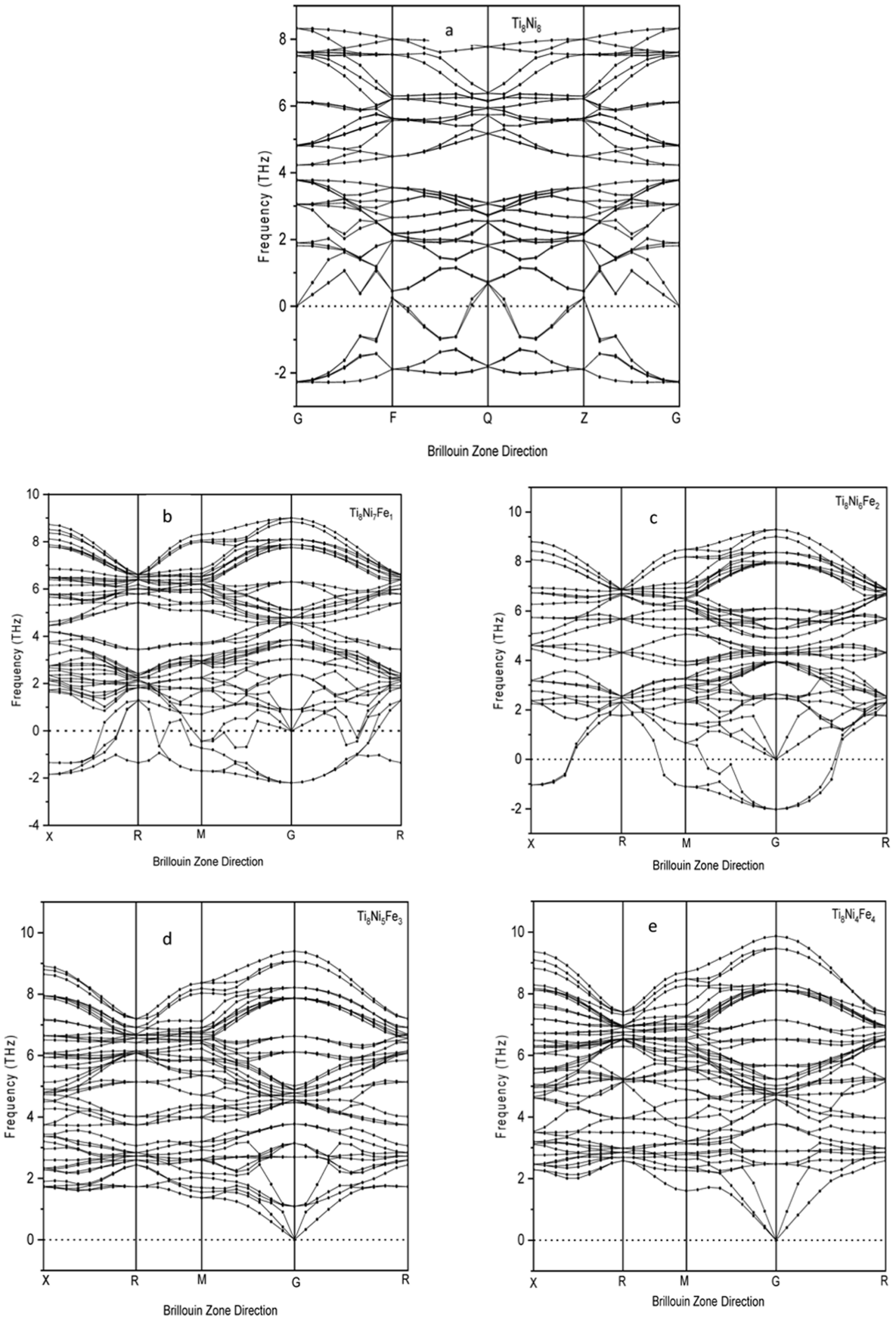

Figure 4. continued

https://doi.org/10.1021/acsomega.4c08953
ACS Omega 2025, 10, 18303−18311

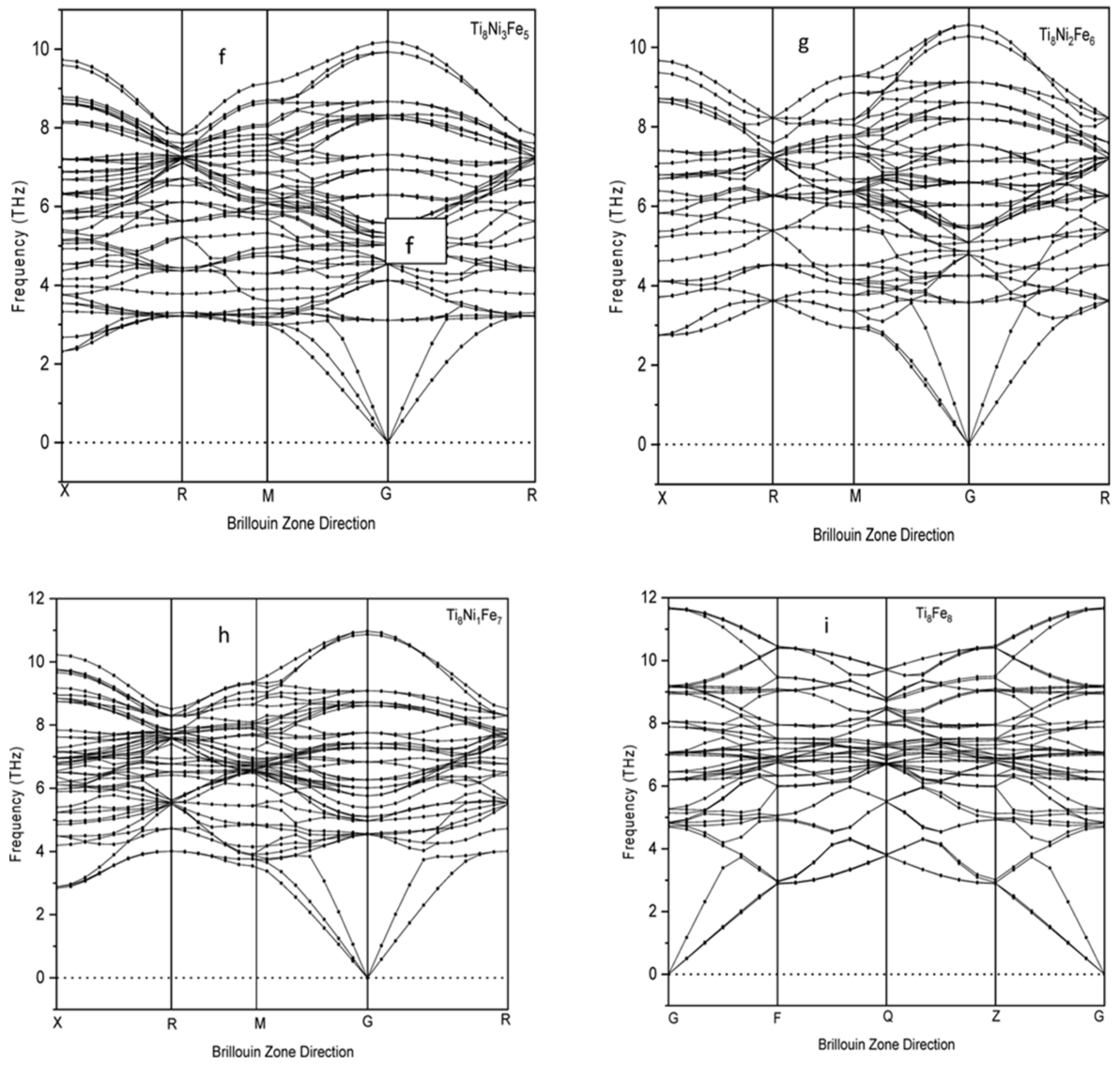

Figure 4. Phonon dispersion for (a) Ti_8Ni_8, (b) $Ti_8Ni_7Fe_1$, (c) $Ti_8Ni_6Fe_2$, (d) $Ti_8Ni_5Fe_3$, (e) $Ti_8Ni_4Fe_4$, (f) $Ti_8Ni_3Fe_5$, (g) $Ti_8Ni_2Fe_6$, (h) $Ti_8Ni_1Fe_7$, and (i) Ti_8Fe_8 alloys.

$Ti_8Ni_{8-x}Fe_x$ (x = 5−8) demonstrated ductile materials. The least ductile alloy is $Ti_8Ni_3Fe_5$ (0.27), and Ti_8Fe_8 (0.27) is the most ductile alloy. According to Pugh,[32] a solid's brittleness or ductility can be determined by dividing its bulk and shear modulus. The G/B ratio has been observed to rise as the Fe content increased, indicating a shift toward more brittle mechanical behavior. The empirical standard necessitates that G/B should be greater than 0.57 for brittle metals and less than 0.57 for ductile materials.[33] $Ti_8Ni_{8-x}Fe_x$ alloys maintained ductile behavior, which is important for biomedical applications.

The hardness of $Ti_8Ni_{8-x}Fe_x$ alloys has been observed to increase with an increased Fe content, suggesting that the wear resistance of the alloys is enhanced. Similar results were obtained elsewhere in the literature.[34,35] Pugh's modulus ratio ($k = G/B$) to express hardness in terms of the polycrystalline modulus was used to determine the Vickers hardness.[36]

$$H_V = 0.92K^{1.137}G^{0.708} \quad (5)$$

It was discovered that the Ti_8Ni_8 structure had a lower hardness value of 0.26, followed by $Ti_8Ni_7Fe_1$ with 1.16, which is significantly smaller compared to other structures. Corresponding with the calculated anisotropy values, $Ti_8Ni_{8-x}Fe_x$ (x = 1−3) structure's estimated universal anisotropy (A^U) value is greater than 0.8, indicating anisotropic.

When Fe is introduced into TiNi alloys, it occupies the substitutional sites of Ni atoms. The magnetic moment is dependent on the neighboring atoms. The magnetic state of Fe in TiNi alloys depends on its concentration. At lower Fe concentrations, the system exhibits paramagnetic behavior, while at higher concentrations, it shows weak ferromagnetic behavior as compared with the magnetic ordering of ML-CrSeO, which has transition metal elements, exhibiting antiferromagnetic behavior at the ground state.[37]

3.3. Density of States. To reveal the interaction between atoms in $Ti_8Ni_{8-x}Fe_x$ (x = 1−3) alloys, the total and partial density of states (TDOS and PDOS) are calculated. Figure 3 shows the TDOS and PDOS for $Ti_8Ni_{8-x}Fe_x$ (x = 1−3) alloys. The stability trend of atomic structures at the Fermi level (E_F) is compared. The structure with the greatest and smallest density of states at E_F is considered the least and most stable,

https://doi.org/10.1021/acsomega.4c08953
ACS Omega 2025, 10, 18303−18311

respectively. The TDOS for the $Ti_8Ni_{8-x}Fe_x$ structures consists of narrow but high d-derived bands, intermediate p-derived bands, and low but broad s-derived bands. The d-states contribute the most to the TDOS, with the s-orbitals contributing the least. Furthermore, the TDOS above the Fermi level is primarily made up of d-states in the Ti site, whereas the TDOS below the Fermi level is primarily made up of d-states contributed by the Ni. The third element contributed very little to the TDOS in the vicinity of the Fermi level; a d−d hybridization between the Ti and Ni sites is indicated by the significant intensity for Ni d-states at lower energies and Ti d-states at higher energies. Ti_8Fe_8 has the lowest energy at E_F and is the most stable, while Ti_8Ni_8 is the least stable, with the highest TDOS at Fermi. Consequently, these alloys' MT temperatures are lower than TiNi's. The TDOS stability trend and heat of formation results showed that Ti_8Fe_8 is thermodynamically stable.

3.4. Phonon Dispersions. Figure 4 displays phonon dispersion curves for $Ti_8Ni_{8-x}Fe_x$ (x = 0−8) alloys. Data have been computed using the PHONON code[38] to ascertain the vibrational stability of the alloys. The phonon dispersion curves are used to study the vibrational stability of the alloys. The absence of soft modes (negative frequencies) across the Brillouin zone indicates that the alloys are stable. The increase in Fe content changed the phonon frequencies due to bonding characteristics between Ni and Fe. The binary B2 Ti_8Ni_8 alloy showed the presence of soft modes, confirming the vibrational instability of the alloy. Negative frequencies have been observed along high symmetry directions in the $Ti_8Ni_7Fe_1$ and $Ti_8Ni_6Fe_2$ phonon curves, demonstrating that the B2 $Ti_8Ni_{8-x}Fe_x$ (x = 1−2) structures are vibrationally unstable. As the Fe content increases, the negative frequencies decrease. For $Ti_8Ni_{8-x}Fe_x$ (x = 3−7), the soft modes disappeared, suggesting that the alloys are vibrationally stable, which validates vibrational stability in line with the predetermined C_{ij}.

In TiNi alloys, the Longitudinal Optical-Transverse Optical (LO-TO) splitting effects are negligible since the alloys exhibit a covalent metallic bond. Consequently, the frequencies of the LO and TO phonon modes at the Γ-point remain degenerate. Compared with the real topological phonons in 3D carbon allotropes, the state at k_2 = 0 has been confirmed to possess double degeneracy.[39] The spin−orbital coupling in TiNi alloys is weakened due to the lack of heavy elements.

4. CONCLUSIONS

In this work, first-principles calculations were used to investigate the lattice parameters, elastic constants, heat of formation, density of states, and phonon dispersion of B2 $Ti_8Ni_{8-x}Fe_x$ (x = 0−8). The obtained lattice parameters were found to be comparable with those of other theoretical and experimental data, indicating the validity of this study. The study further discovered that the addition of Fe contents reduced the structure formation of heat. The heat of formation decreases with the rising Fe concentration. The addition of Fe enhances the C' value and increase C_{11}, C_{44}. As Fe content increases, the anisotropy value decreases. The shear modulus increases with the addition of Fe atoms. The TDOS and PDOS revealed the thermodynamic stability of Ti_8Fe_8 alloys. Phonon dispersion provides insights into vibrational stability, phase transition, and mechanical properties of $Ti_8Ni_{8-x}Fe_x$ (x = 0−8) alloys. This enables the development of devices for biomedical applications. Phonon dispersion calculations on $Ti_8Ni_{8-x}Fe_x$ (x = 0−2) structures at room temperature indicated the unstable condition of the alloys. The composition with Fe content (x = 3−7) shows stable phonon spectra, with no soft modes. This suggests that these alloys are thermodynamically favorable. The Fe atom substitution improved the mechanical properties such as stiffness and strength, minimizing the stress shielding of implants and stents with natural tissue. The addition of iron to TiNi alloys has altered the SME and superelasticity of TiNi. However, for biomedical applications, further research needs to be done to decrease Young's modulus of these materials to match that of bone or tissue.

■ ASSOCIATED CONTENT

Supporting Information

The Supporting Information is available free of charge at https://pubs.acs.org/doi/10.1021/acsomega.4c08953.

All calculations were performed using Density Functional Theory (DFT) with the generalized gradient approximation (GGA) of Perdew, Burke, and Ernzerhof (PBE). The purpose of this study was to investigate the impact of substituting Ni with Fe on the shape memory properties of TiNi alloy using a first-principles methodology for biomedical applications (PDF)

■ AUTHOR INFORMATION

Corresponding Author

Thabiso Mathews − *Department of Physics, Sefako Makgatho Health Sciences University, 0204 Pretoria, South Africa;* orcid.org/0000-0001-8562-432X; Email: mathewsthabisoabel@gmail.com

Authors

Enoch Sithole − *Department of Physics, Sefako Makgatho Health Sciences University, 0204 Pretoria, South Africa;* orcid.org/0000-0003-4454-4109

Rosinah Modiba − *Department of Physics, Sefako Makgatho Health Sciences University, 0204 Pretoria, South Africa; Advanced Materials Engineering, Manufacturing Cluster, CSIR, Council for Scientific and Industrial Research, 0001 Pretoria, South Africa*

Mandy Madigoe − *Advanced Materials Engineering, Manufacturing Cluster, CSIR, Council for Scientific and Industrial Research, 0001 Pretoria, South Africa*

Complete contact information is available at: https://pubs.acs.org/10.1021/acsomega.4c08953

Author Contributions

Mathews T: performed first-principle calculations, data collection, and drafted the manuscript. Sithole E and Modiba R: supervision, contribution to the conception and design of the study, reviewing, and editing. Madigoe M: data collection and discussed results. All authors have agreed to the published version of the manuscript.

Notes

The authors declare no competing financial interest.

■ ACKNOWLEDGMENTS

The author would like to thank Sefako Makgatho Health Sciences University for its support and the assistance of colleagues at the Council for Scientific and Industrial Research in Pretoria. Calculations and simulations were performed using a High-Performance Computing center in Cape Town.

REFERENCES

(1) Liang, Q.; Zhao, S.; Liang, C.; Zhao, T.; Wang, D.; Ding, X.; Li, S.; Wang, Y.; Zheng, Y.; Ren, X.; Mills, M. J.; Wang, Y. Strain states and unique properties in cold-rolled TiNi shape memory alloys. *Acta Mater.* **2022**, *231*, 117890.

(2) Gloanec, A.-L.; Bilotta, G.; Gerland, M. Deformation mechanisms in a TiNi shape memory alloy during cyclic loading. *Mater. Sci. Eng., A* **2013**, *564*, 351−358.

(3) Li, H.; Sun, D.; Cai, X.; Dong, P.; Gu, X. Laser welding of TiNi shape memory alloy and stainless steel using Co filler metal. *Opt Laser. Technol.* **2013**, *45*, 453−460.

(4) Zhang, C.; He, L.; Chen, Y.; Dai, D.; Su, Y.; Shao, L. Corrosion Behavior and In Vitro Cytotoxicity of NiTi and Stainless Steel Arch Wires Exposed to Lysozyme, Ovalbumin, and Bovine Serum Albumin. *ACS Omega* **2020**, *5* (30), 18995−19003.

(5) Ishii, A. Elastic investigation for the existence of B33 phase in TiNi shape memory alloys using atomistically informed Eshelby's ellipsoidal inclusion. *Comput. Mater. Sci.* **2023**, *218*, 111954.

(6) Kadkhodaei, S.; van de Walle, A. First-principles calculations of thermal properties of the mechanically unstable phases of the PtTi and NiTi shape memory alloys. *Acta Mater.* **2018**, *147*, 296−303.

(7) Li, G.; Chi, W.; Wang, W.; Liu, X.; Tu, H.; Long, X. High cycle fatigue behavior of additively manufactured Ti-6Al-4V alloy with HIP treatment at elevated temperatures. *Int. J. Fatig.* **2024**, *184*, 108287.

(8) Yuan, B.; Zhu, M.; Chung, C. Y. Biomedical Porous Shape Memory Alloys for Hard-Tissue Replacement Materials. *Materials* **2018**, *11* (9), 1716.

(9) Zhu, Z.; Guo, D.; Xu, J.; Lin, J.; Lei, J.; Xu, B.; Wu, X.; Wang, X. Processing Characteristics of Micro Electrical Discharge Machining for Surface Modification of TiNi Shape Memory Alloys Using a TiC Powder Dielectric. *Micromachines* **2020**, *11* (11), 1018.

(10) Lin, L. W.; Wang, H.; Ni, M.; Rui, Y.; Cheng, T.-Y.; Cheng, C.-K.; Pan, X.; Li, G.; Lin, C. Enhanced osteointegration of medical titanium implant with surface modifications in micro/nanoscale structures. *J. Orthop. Transl.* **2014**, *2* (1), 35−42.

(11) Hsieh, S.-F.; Wu, S. K.; Lin, H.-Y. Transformation temperatures and second phases in Ti−Ni−Si ternary shape memory alloys with Si ≤ 2 at.%. *J. Alloys Compd.* **2002**, *339* (1−2), 162−166.

(12) Pushin, V.; Kuranova, N.; Marchenkova, E.; Pushin, A. Design and Development of Ti−Ni, Ni−Mn−Ga and Cu−Al−Ni-based Alloys with High and Low Temperature Shape Memory Effects. *Materials* **2019**, *12* (16), 2616.

(13) Miura, K.; Yamada, N.; Hanada, S.; Jung, T.-K.; Itoi, E. The bone tissue compatibility of a new Ti−Nb−Sn alloy with a low Young's modulus. *Acta Biomater.* **2011**, *7* (5), 2320−2326.

(14) Hao, Y. L.; Zhang, Z. B.; Li, S. J.; Yang, R. Microstructure and mechanical behavior of a Ti−24Nb−4Zr−8Sn alloy processed by warm swaging and warm rolling. *Acta Mater.* **2012**, *60* (5), 2169−2177.

(15) Li, Y. Y.; Zou, L. M.; Yang, C.; Li, Y. H.; Li, L. J. Ultrafine-grained Ti-based composites with high strength and low modulus fabricated by spark plasma sintering. *Mater. Sci. Eng., A* **2013b**, *560*, 857−861.

(16) Payne, M. C.; Teter, M. P.; Allan, D. C.; Arias, T. A.; Joannopoulos, J. D. Iterative minimization techniques for ab initio total-energy calculations: molecular dynamics and conjugate gradients. *Rev. Mod. Phys.* **1992**, *64* (4), 1045−1097.

(17) Clark, S. J.; Segall, M. D.; Pickard, C. J.; Hasnip, P. J.; Probert, M. I. J.; Refson, K.; Payne, M. C. First principles methods using CASTEP. *Z. Kristallogr.* **2005**, *220* (5−6), 567−570.

(18) Perdew, J. P.; Burke, K.; Ernzerhof, M. Generalized Gradient Approximation Made Simple. *Phys. Rev. Lett.* **1996**, *77* (18), 3865−3868.

(19) Liang, Y. F.; Shang, S. L.; Wang, J.; Wang, Y.; Ye, F.; Lin, J. P.; Chen, G. L.; Liu, Z. K. First-principles calculations of phonon and thermodynamic properties of Fe-Si compounds. *Intermetallics* **2011**, *19* (10), 1374−1384.

(20) Wang, Z.; Ning, Y.; Di, P.; Zhang, B.; Yu, H.; Xie, B. Understanding the fracture mechanisms of Ni−Co−Cr-type superalloys: Role of precipitate evolution and strength degradation. *Mater. Sci. Eng., A* **2024**, *902*, 146623.

(21) Zhao, Y. Stability of phase boundary between L12-Ni3Al phases: A phase field study. *Intermetallics* **2022**, *144*, 107528.

(22) Zhang, Z.; Elkedim, O.; Ma, Y. Z.; Balcerzak, M.; Jurczyk, M. The phase transformation and electrochemical properties of TiNi alloys with Cu substitution: Experiments and first-principle calculations. *Int. J. Hydrogen Energy* **2017**, *42* (2), 1444−1450.

(23) Li, X.; Tu, X.; Liu, B.-Q.; Song, J.; Luo, W.; Lei, Y.; Sun, G.; Chen, B.; Hu, Q.-M. Composition-dependent elastic properties in TiNi-Nb from first principle calculations. *J. Alloys Compd.* **2017**, *706*, 260−266.

(24) Baloyi, M. E.; Modiba, R. M.; Ngoepe, P. E.; Chauke, H. *Structural, Elastic and Electronic Properties of Binary Titanium-Based Shape Memory Slloys*; SAIP Proceedings, 2019.

(25) Otsuka, K.; Sawamura, T.; Shimizu, K. Crystal structure and internal defects of equiatomic TiNi martensite. *Phys. Status Solidi A* **1971**, *5* (2), 457−470.

(26) Ngobe, B.; Molepo, M.; Phasha, M. First-principles study on the effect of Ni addition on the stability of B2 $Ti_{50}Ru_{50}$ − a supercell approach. *MATEC Web Conf.* **2023**, *388*, 07017.

(27) Li, Y.; Gao, Y.; Xiao, B.; Min, T.; Fan, Z.; Ma, S.; Xu, L. Theoretical study on the stability, elasticity, hardness and electronic structures of W−C binary compounds. *J. Alloys Compd.* **2010**, *502* (1), 28−37.

(28) Ren, X.; Otsuka, K. The Role of Softening in Elastic Constant c44 in Martensitic Transformation. *Scr. Mater.* **1998**, *38* (11), 1669−1675.

(29) Gschneidner, K. A.; Russell, A. J.; Pecharsky, A. O.; Morris, J.; Zhang, Z.-H.; Lograsso, T. A.; Hsu, D.; Chester Lo, C. H.; Ye, Y.; Slager, A.; Kesse, D. A family of ductile intermetallic compounds. *Nat. Mater.* **2003**, *2* (9), 587−591.

(30) Kanoun, M. B.; Goumri-Said, S.; Jaouen, M. Structure and mechanical stability of molybdenum nitrides: A first-principles study. *Phys. Rev. B: Condens. Matter Mater. Phys.* **2007**, *76* (13), 134109.

(31) Hua, L.; Liu, Y.; Qian, D.; Xie, L.; Wang, F.; Wu, M. Mechanism of void healing in cold rolled aeroengine M50 bearing steel under electroshocking treatment: A combined experimental and simulation study. *Mater. Charact.* **2022**, *185*, 111736.

(32) Pugh, S. F. XCII. Relations between the elastic moduli and the plastic properties of polycrystalline pure metals. *London, Edinburgh Dublin Philos. Mag. J. Sci.* **1954**, *45* (367), 823−843.

(33) Schiltz, R. J.; Smith, J. F. Elastic constants of some *M*Al2 single crystals. *J. Appl. Phys.* **1974**, *45* (11), 4681−4685.

(34) Zhang, D.; Shi, D.; Wang, F.; Qian, D.; Zhou, Y.; Fu, J.; Chen, M.; Qiu, D.; Jiang, S. Electromagnetic shocking induced fatigue improvement via tailoring the α-grain boundary in metastable β titanium alloy bolts. *J. Alloys Compd.* **2023**, *966*, 171536.

(35) Shao, L.; Zhang, X.; Chen, Y.; Zhu, L.; Wu, S.; Liu, Q.; Li, W.; Xue, N.; Tu, Z.; Wang, T.; et al. Why do cracks occur in the weld joint of Ti-22Al-25Nb alloy during post-weld heat treatment? *Front. Mater.* **2023**, *10*, 1135407.

(36) Ranganathan, S. I.; Ostoja-Starzewski, M. Universal Elastic Anisotropy Index. *Phys. Rev. Lett.* **2008**, *101* (5), 055504.

(37) Gong, J.; Wang, Y.; Han, Y.; Cheng, Z.; Wang, X.; Yu, Z.; Yao, Y. Hidden real topology and unusual magnetoelectric responses in two-dimensional antiferromagnets. *Adv. Mater.* **2024**, *36*, 2402232.

(38) Parlinski, K.; Li, Z. Q.; Kawazoe, Y. First-Principles Determination of the Soft Mode in CubicZrO_2. *Phys. Rev. Lett.* **1997**, *78* (21), 4063−4066.

(39) Wang, X.; Bai, J.; Wang, J.; Cheng, Z.; Qian, S.; Wang, W.; Zhang, G.; Yu, Z.; Yao, Y. Real topological phonons in 3D carbon allotropes. *Adv. Mater.* **2024**, *36*, 202407437.

https://doi.org/10.1021/acsomega.4c08953
ACS Omega 2025, 10, 18303−18311